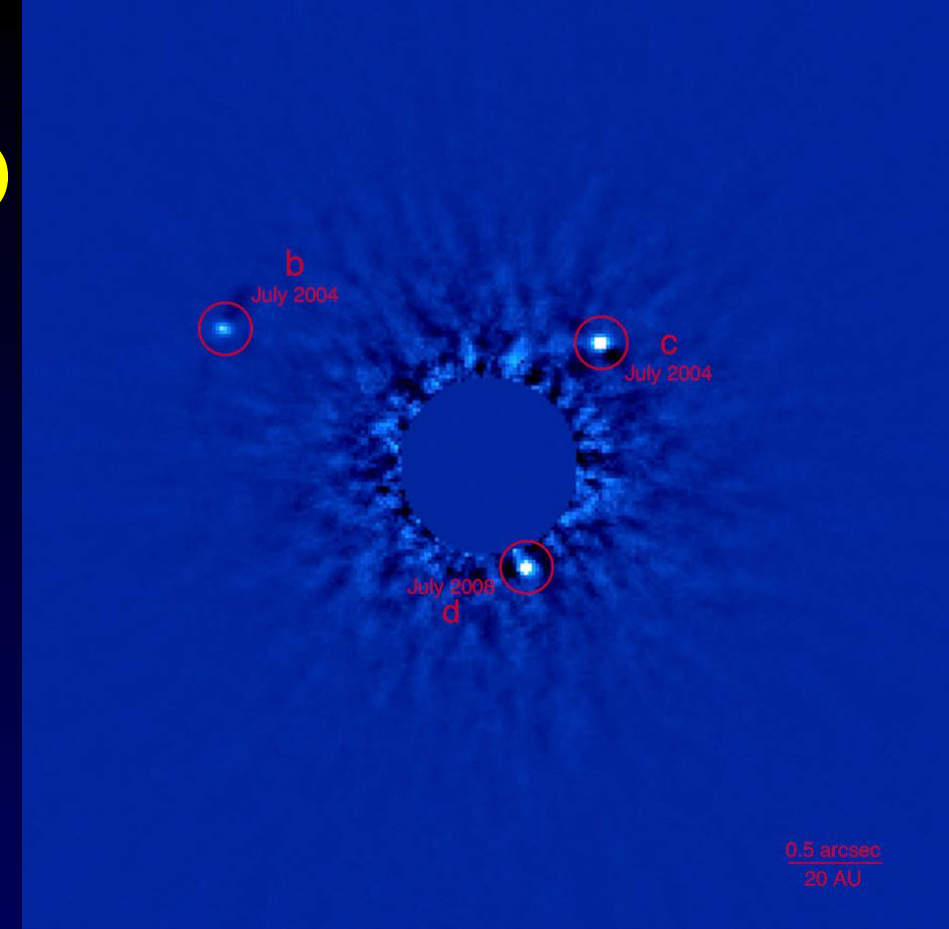


Different AO Flavours

Method	Acronym	Field of View
Natural Guide Star AO	SCAO	<10" (10 arcsec)
Laser Tomographic AO	LTAO	Tens of arcsec
Multi-Object AO	MOAO	N × tens of arcsec
Multi-Conjugate AO	MCAO	≤ about 2' (2 arcmin)
Ground Layer AO	GLAO	Upto 10' (10 arcmin)
Extreme AO	XAO	<10" (10 arcsec)

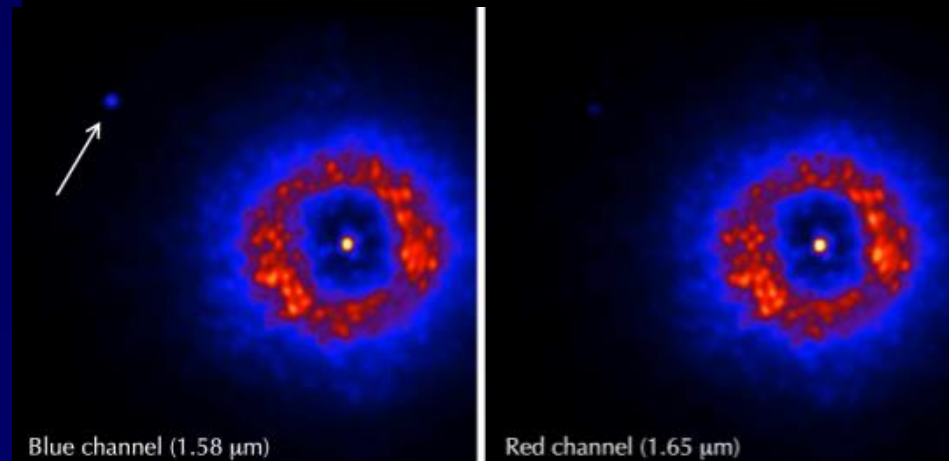
Challenges of AO

- Improved resolution, sharper images, but quite variable temporally and spatially, so calibration is tricky
- MCAO helps but is not widely available
- Uncorrected modes may still be significant, and often techniques such as Angular or Spectral Differential imaging are used to improve the subtraction of these effects (ADI or SDI).
- AO may be used with a coronagraph to suppress the light from the host star



Gemini Observatory / NRC / AURA / Christian Marois, et al.

Gemini Observatory Legacy Image

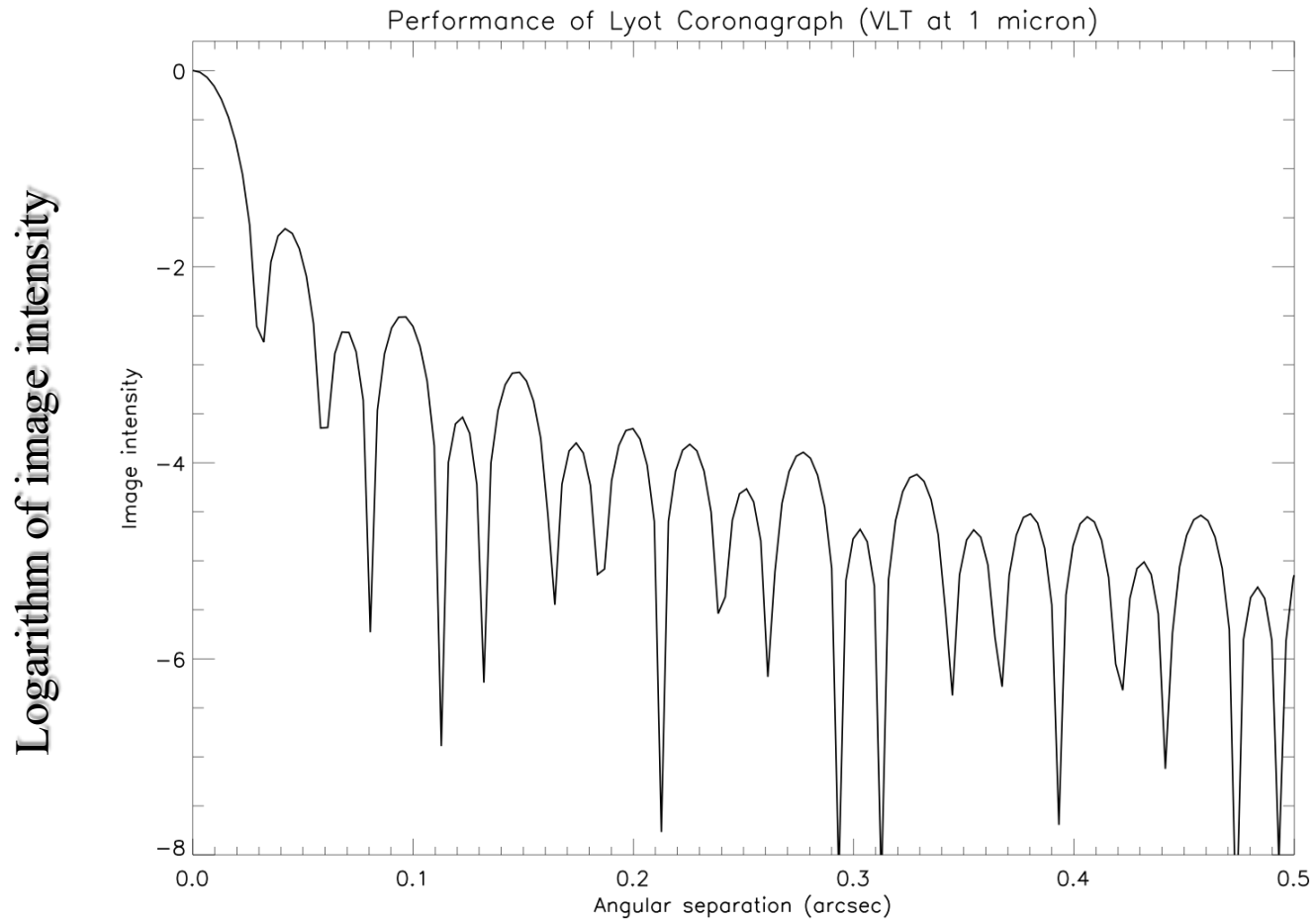


The pale blue dot



Picture taken by Voyager 1 probe looking back at the Sun from 40.5AU

Contrast curve with perfect Strehl

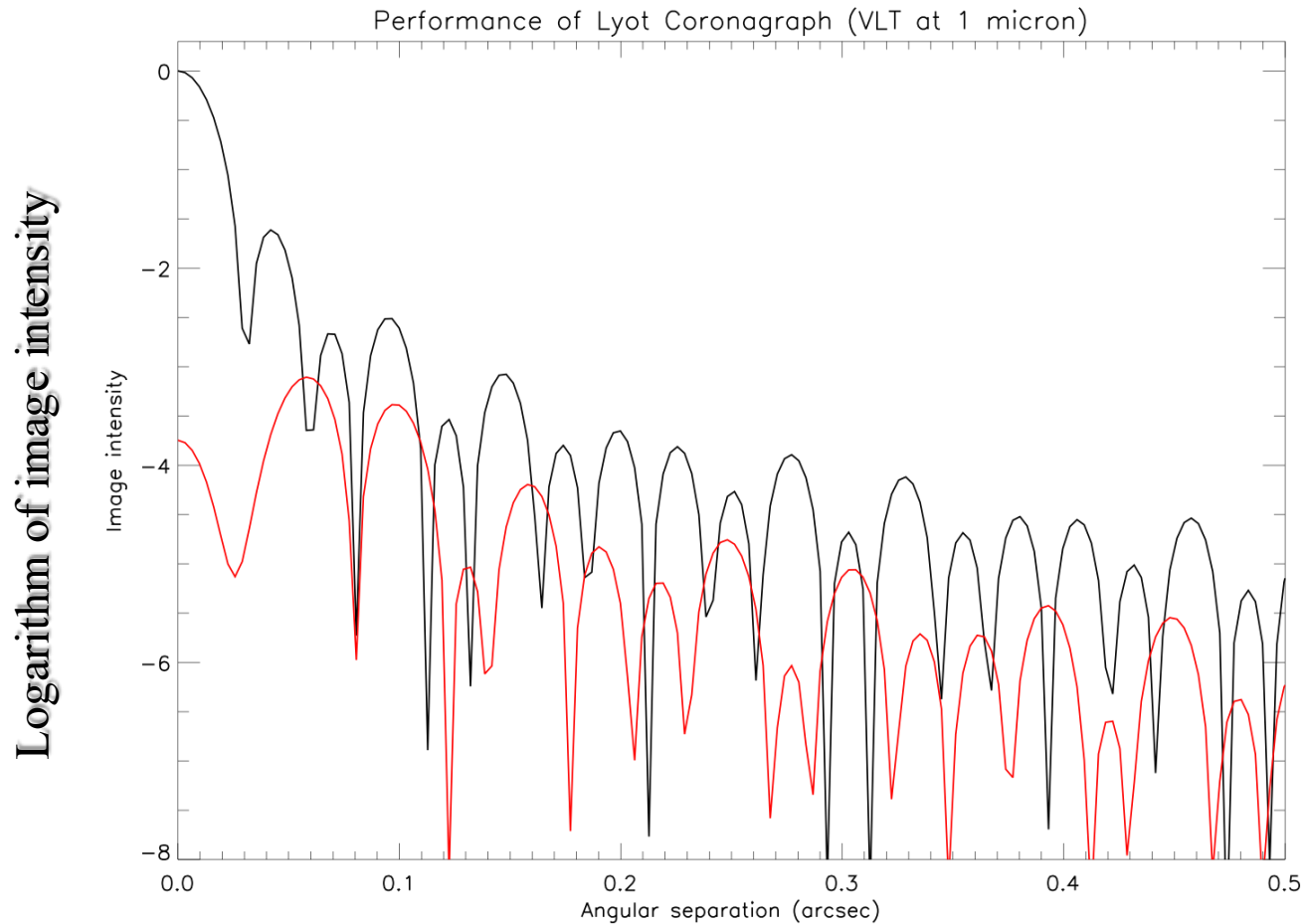


Coronagraphs

- Start with plane wavefront incident at telescope primary (pupil plane)
- Corresponding focal plane image is that of a perfect point source (Airy pattern with central obscuration)
- Introducing focal plane mask that blocks out peak of starlight
- Sharp edge leads to diffracted light at edges of pupil
- Lyot stop in pupil plane masks diffracted light
- Final image has much reduced intensity of starlight, planet unaffected except for small transmission loss.



Contrast curve for Lyot coronagraph

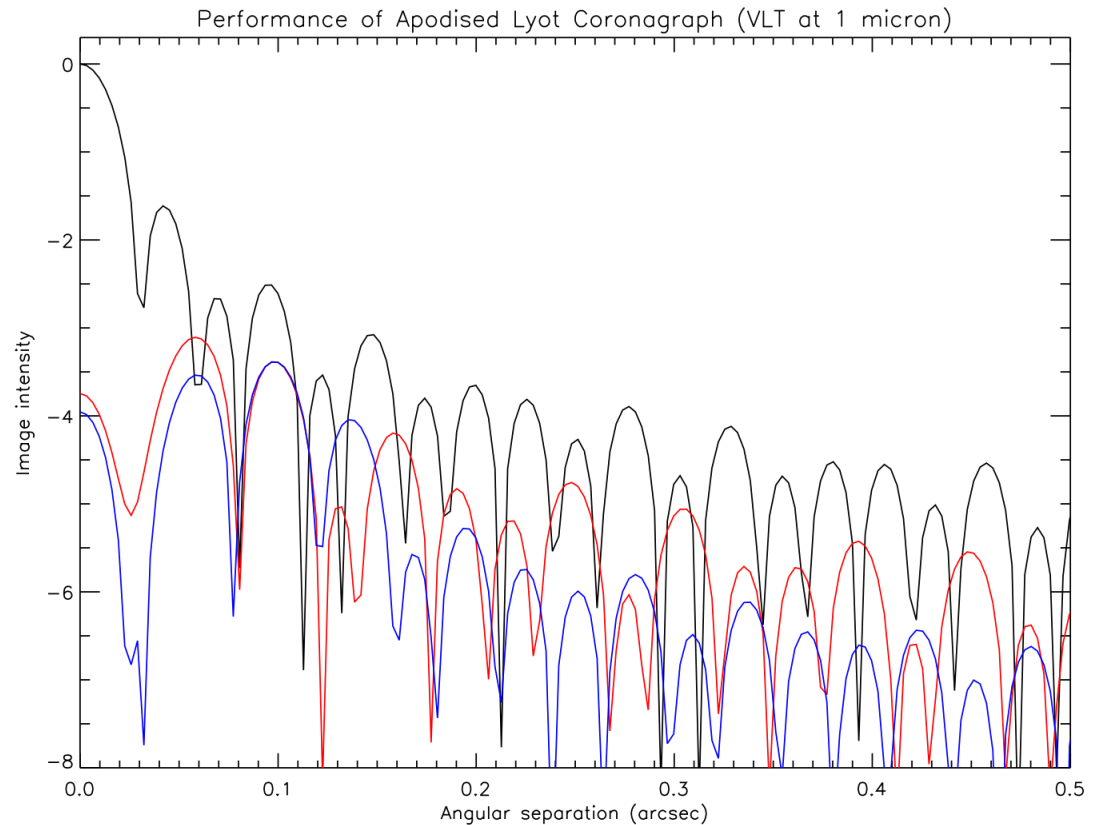


- Hard edges at pupil cause high spatial frequency “ripples”, which lead to lower contrast

Apodisation



- Solution: modify pupil plane distribution to remove all hard edges (Gaussian profile) - technique called apodisation
- Apodised Lyot coronagraph further improves achievable contrast.



ADI (Angular Differential Imaging) + SDI (Spectral Differential Imaging)

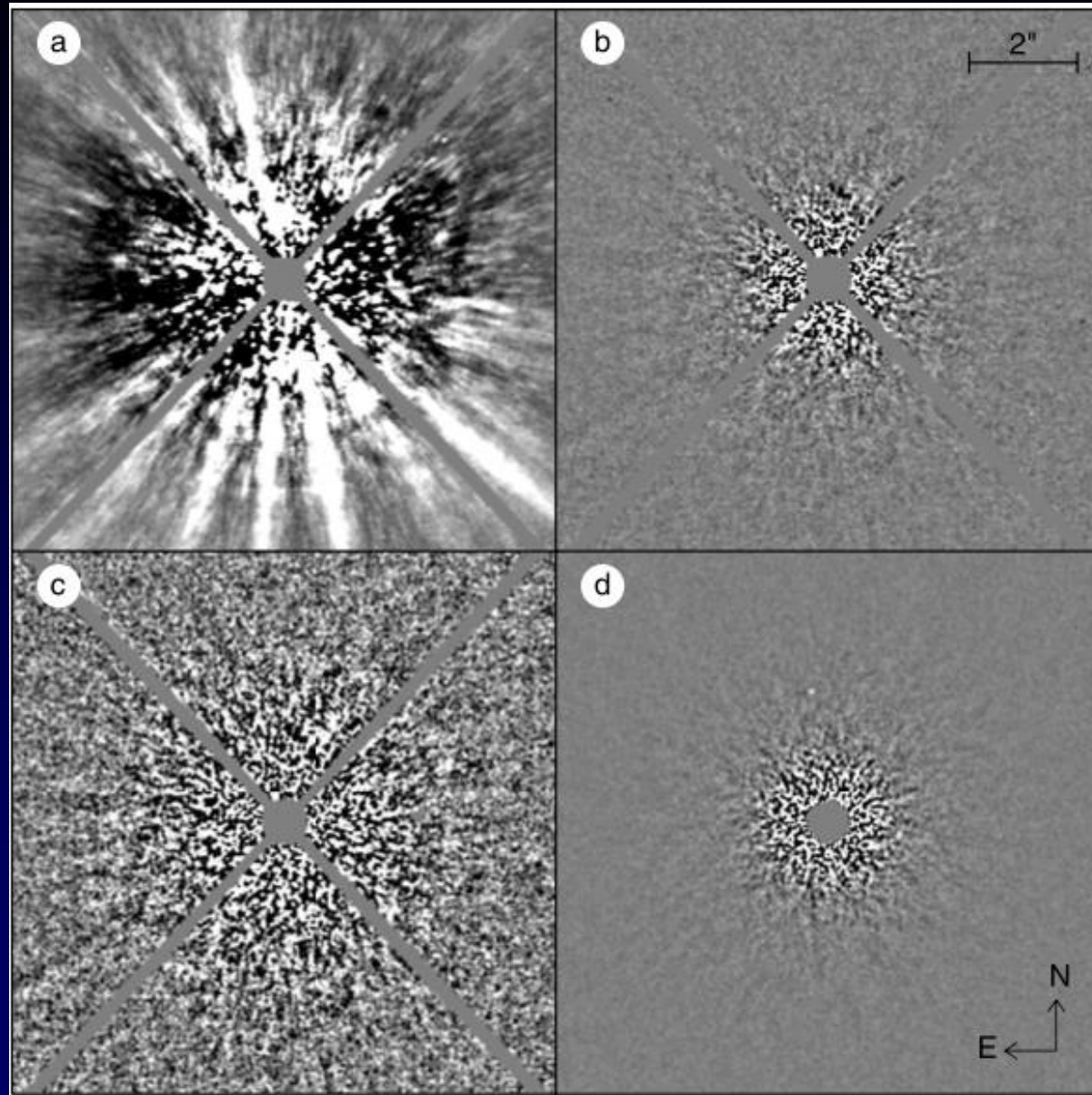
- Residual image structure is partially due to aberrations in the telescope and instrument and uncorrected atmospheric structure
- In Angular Differential Imaging, a sequence of many exposures of the target is acquired using an altitude/azimuth telescope with the instrument rotator turned off (at the Cassegrain focus) to keep instrument and telescope optics aligned.
- This is a very stable configuration and ensures a high correlation of the sequence of PSF images, which would be smeared out if the rotator was used.
- The FOV rotates during the sequence, which has to be allowed for after subtraction of a reference image.
- Spectral Differential Imaging uses images obtained simultaneously on and off a spectral feature (e.g. the 1.6 μ m methane absorption) where the aberrations are highly correlated because they are very close in wavelength
- Spectral deconvolution can be applied to spectrally dispersed Integral Field images (e.g. Thatte et al 2007). Here speckles and other aberrations increase in distance as a function of wavelength because of the increasing diffraction angle, but the separation of an object from its host star is at a fixed distance.

ADI illustrated with Gemini NIRI/Altair 1.6 μ m observations (Lafreniere et al 2007)

(a) Original 30s image of the young star HD 691 after subtraction of an azimuthally symmetric median intensity profile.

(b and c) Corresponding residual image after ADI subtraction using the LOCI algorithm. . Display intensity ranges are 5×10^{-6} and 10^{-6} of stellar PSF peak for the top and bottom rows, respectively

(d) Median combination of 117 such residual images. Each panel is $10''$ on a side. The diffraction spikes from the secondary mirror support vanes and the central saturated region are masked. The faint point source visible in (d) at separation of $2.43''$ could not have been detected without ADI processing.



Spectral Deconvolution

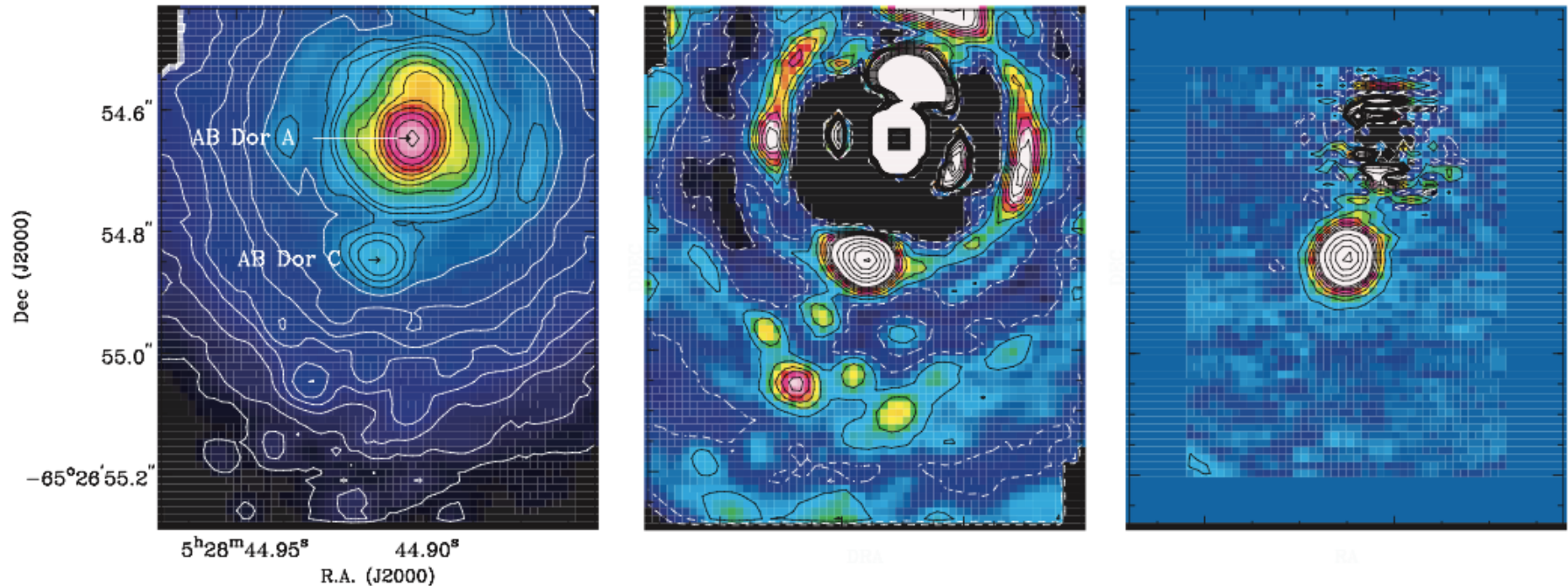
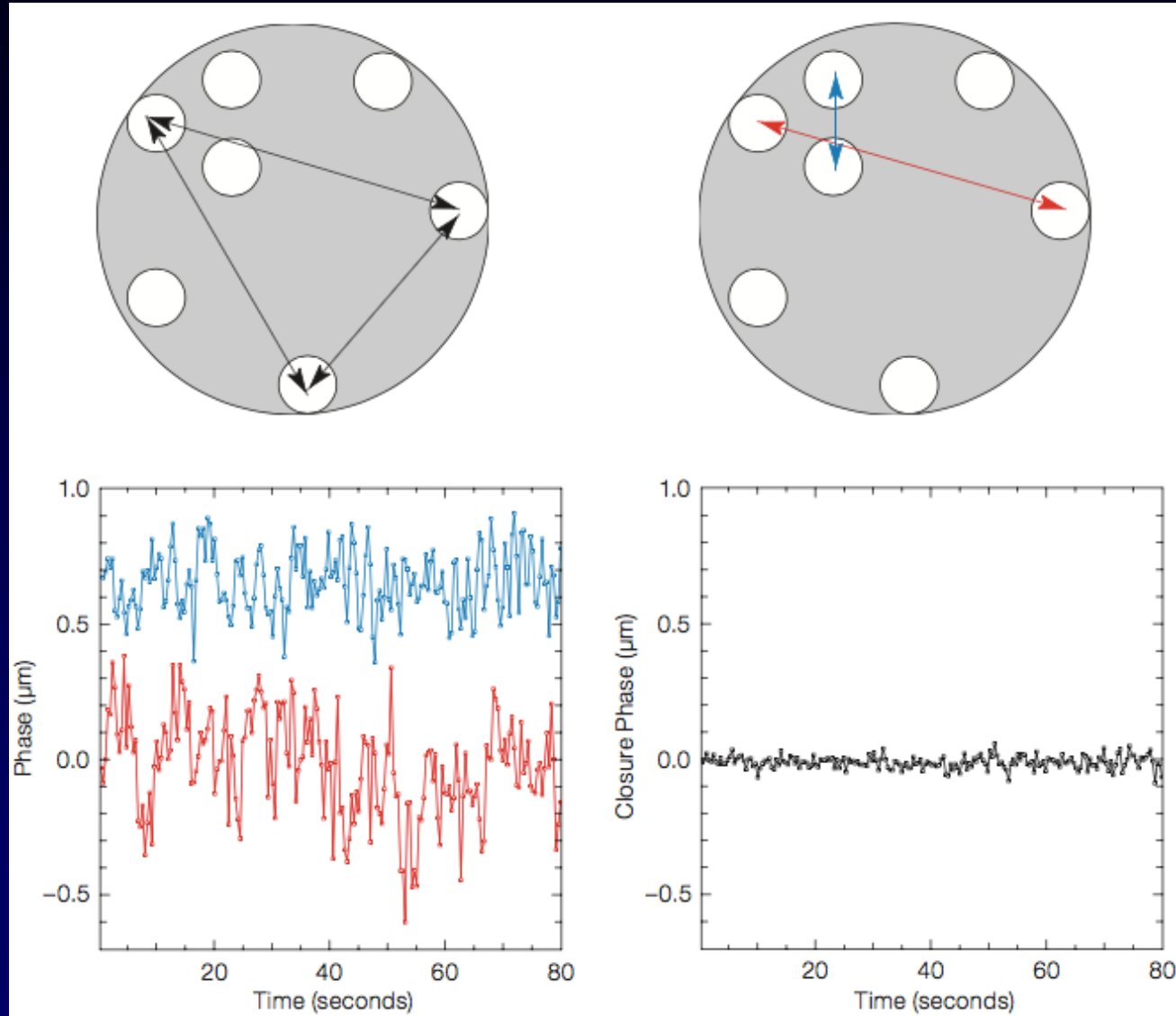


Figure 2. Illustration showing the efficacy of the SD technique at removing both PSF artefacts and super-speckles from the SINFONI IFS data cube for the AB Dor system. The left-hand frame shows one wavelength slice of the observed data cube at 2.2 μm. Note that the entire vertical extent of the image is only 0.9 arcsec. The colour table is logarithmic (minimum 10¹, maximum 10⁴). The contours are logarithmic, from 0.9 to 2.3 in steps of 0.1, and from 2.3 to 4.0 in steps of 0.2. The middle frame shows the same data, but with a radial profile fitted and subtracted, so as to highlight the PSF imperfections. The super-speckles are easily confused with real sources in this narrow-band image. The colour table is now linear (minimum -10, maximum 25), with contours from -12.5 to 32.5 in steps of 5, and from 32.5 to 150 in steps of 20. The four-fold symmetry of the Airy pattern arises from the superposition of the diffraction spikes of the secondary support structure on the Airy rings. The right-hand frame shows the same wavelength slice of the data cube, after applying the SD technique iteratively. Colour table and contours are the same as for the middle frame. Super-speckles are completely absent at the lowest contour level of ±2.5, corresponding to a 1σ error of ≤1 unit.

Thatte et al 2007

Sparse Aperture Mask Interferometry

Phase differences from a mask in NACO on the VLT data are shown in the lower left panel for two different pairs of holes (red and blue baselines, marked on the pupil image), exhibiting phase residuals of ~ 300 nm. In the lower right panel, the closure phase - the sum of three phases of three baselines formed by three separate holes (the triangle is given by black arrows in the pupil image) is given. Most of the phase noise from uncorrected seeing disappears, leaving a closure phase residual of 10 nm; an improvement by a factor of 30.

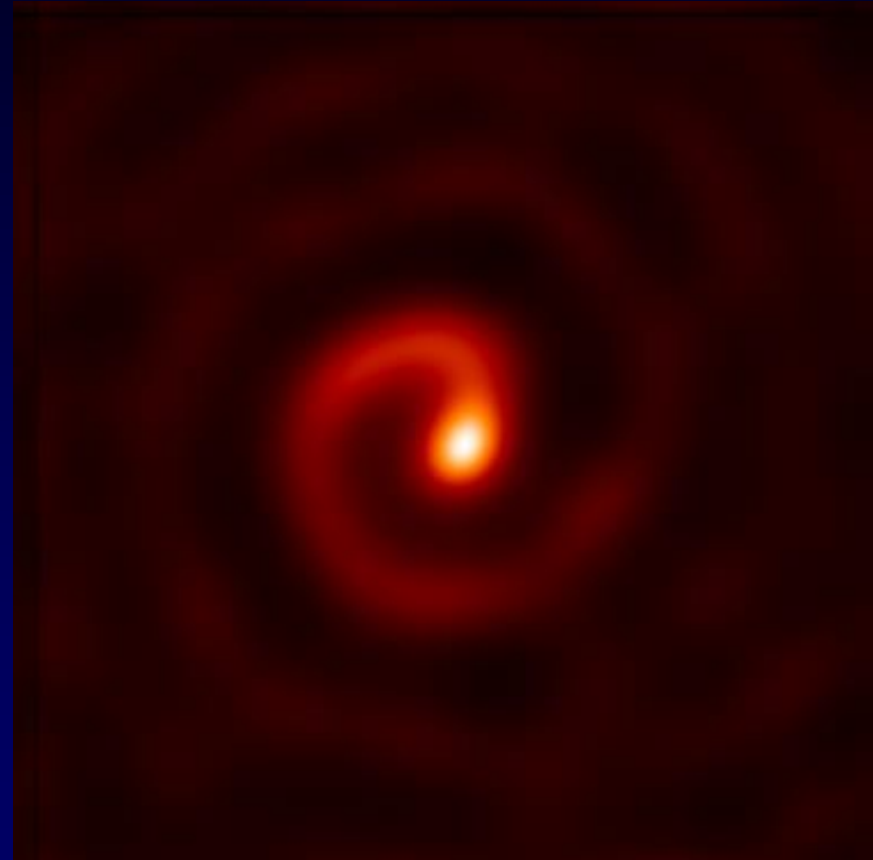


. (Lacour et al 2011)

Sparse Aperture Masking

SAM uses only a fraction of the light collected by the telescope, but provides enhanced stability and resolution, making it suitable for bright objects on large telescopes

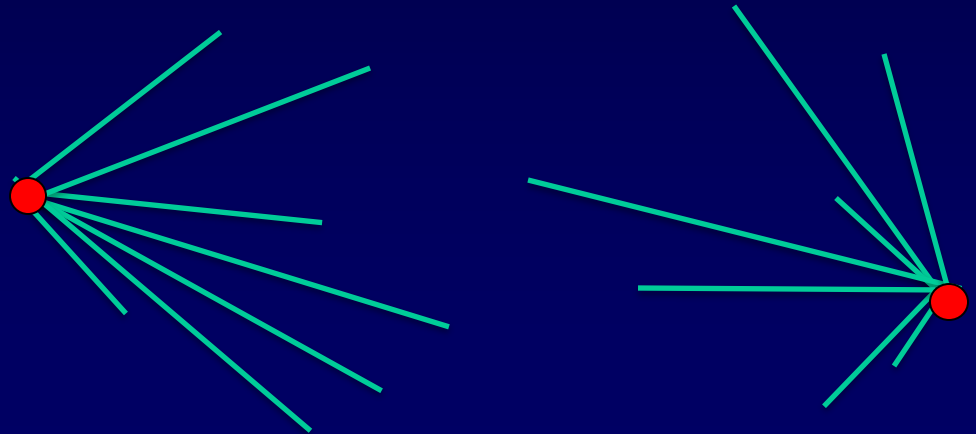
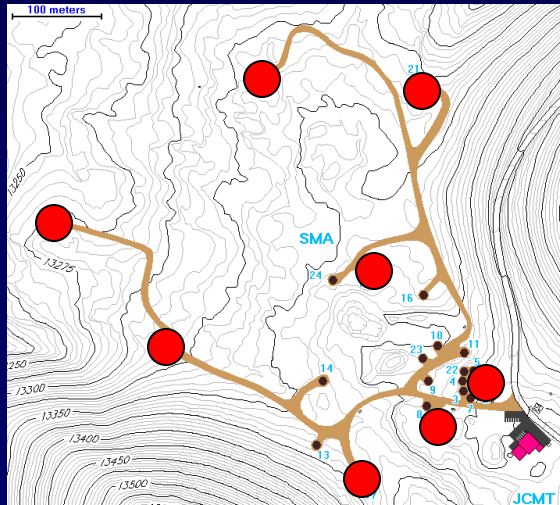
This movie shows a sequence of 11 images of WR104, a late type dusty binary W-R star system obtained on the Keck 10-m telescope in the K-band. (P Tuthill et al 2008)



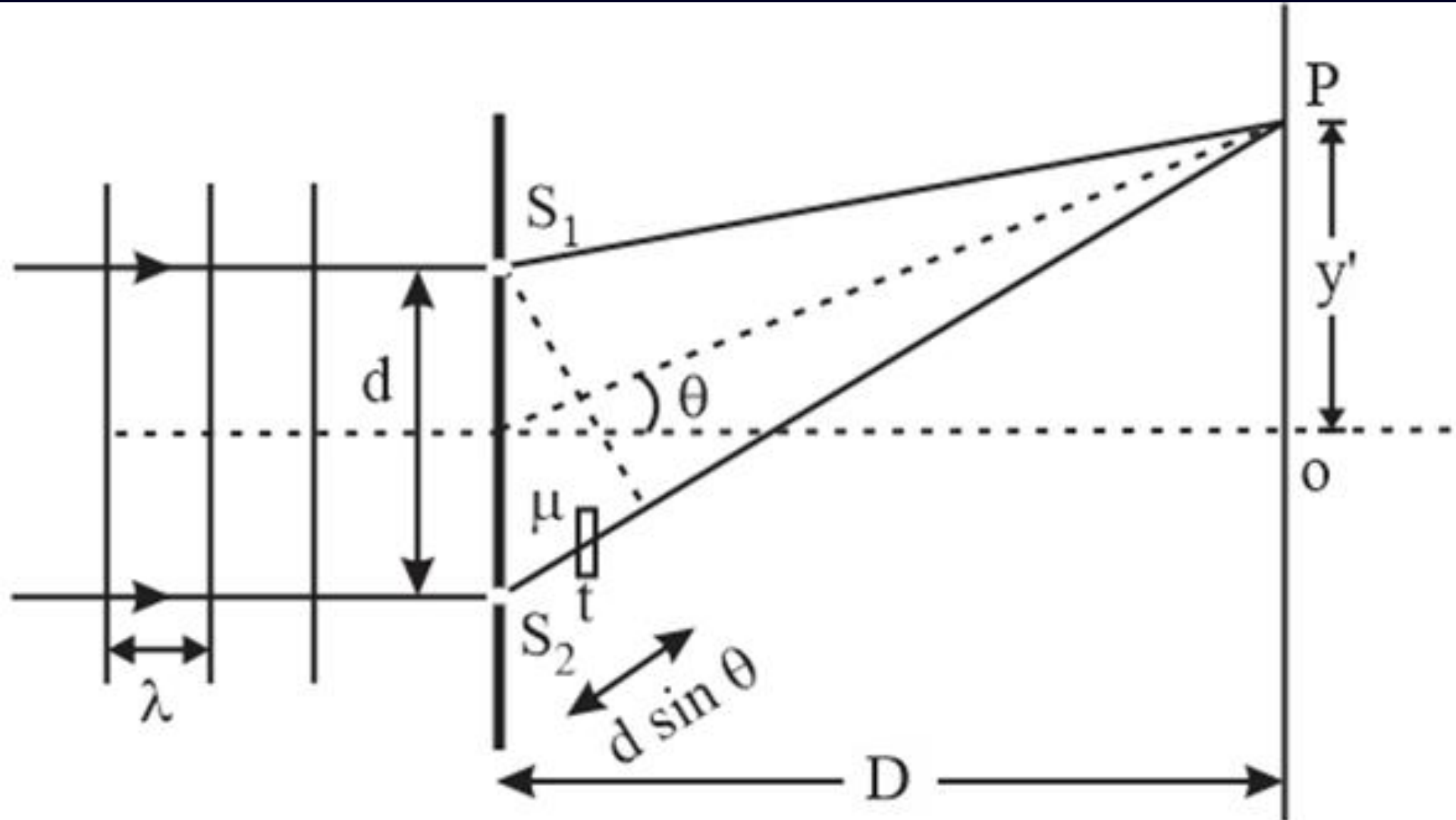
0.4 arcsec

Simulating a large telescope

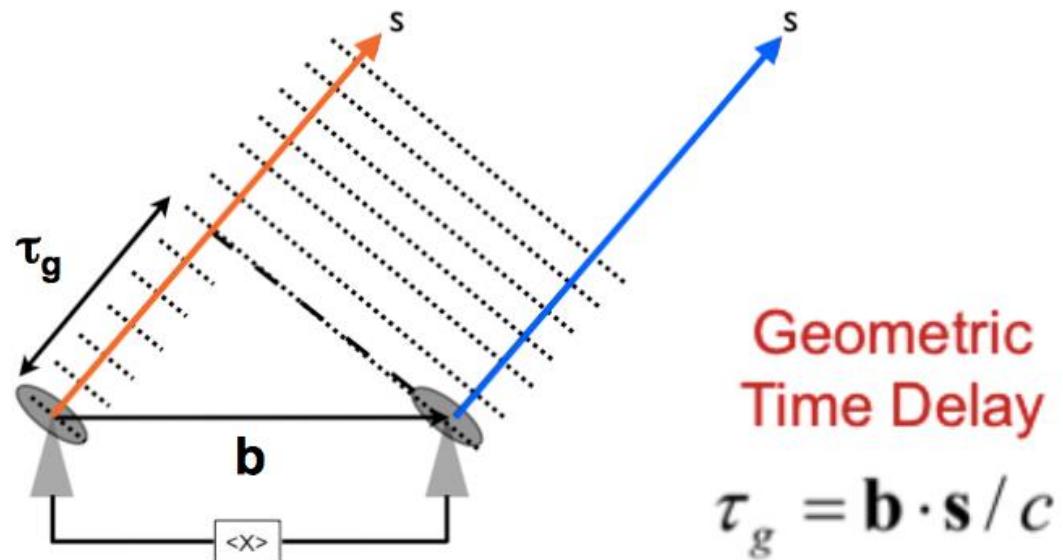
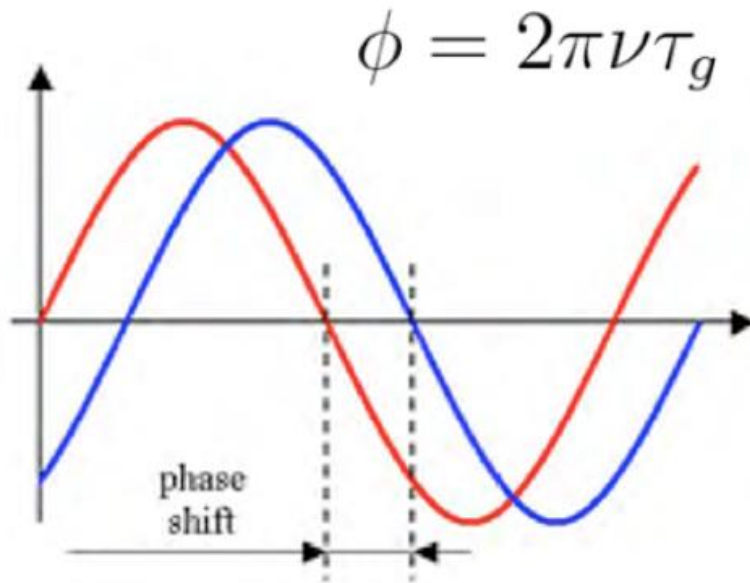
- Arrange a discrete number of telescopes spread out over an area to cover the baselines of interest.
- 1 pair of telescopes \rightarrow 1 baseline sensitive to a particular angular scale
- N telescopes \rightarrow number of samples = $N(N-1)/2$
- As the Earth rotates the projected separation of the telescopes changes
- Sir Martin Ryle, (Cambridge) was awarded the 1974 Nobel Prize in Physics for developing Aperture Synthesis for radio astronomy



Young's Double Slit (in reverse)



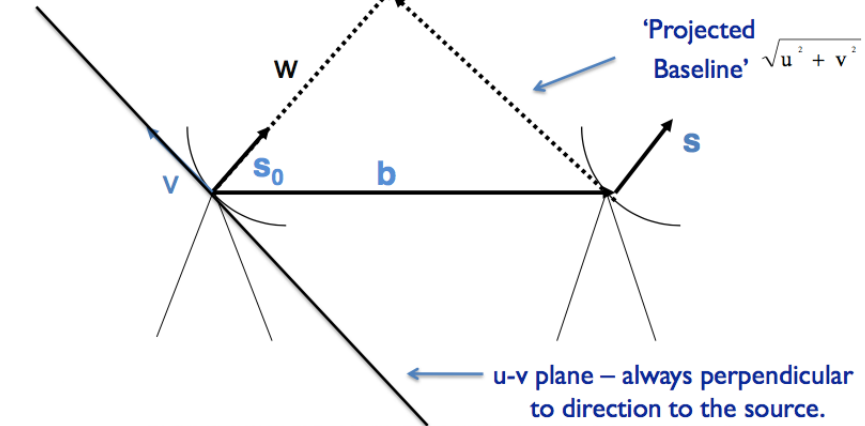
Interferometer Geometric Delay



Because the telescopes are at different positions, the signal from an astronomical source arrives at different times. The geometric delay that arises from the physical separation of the telescopes or antennas has to be accounted for. This delay changes constantly as the Earth rotates.

Interferometry

- This is the coordinate system in most general use for synthesis imaging.
- w points to, and follows the source, u towards the east, and v towards the north celestial pole. The direction cosines l and m then increase to the east and north, respectively.

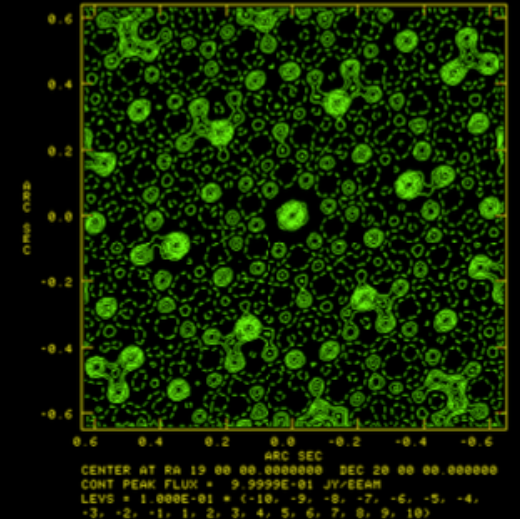
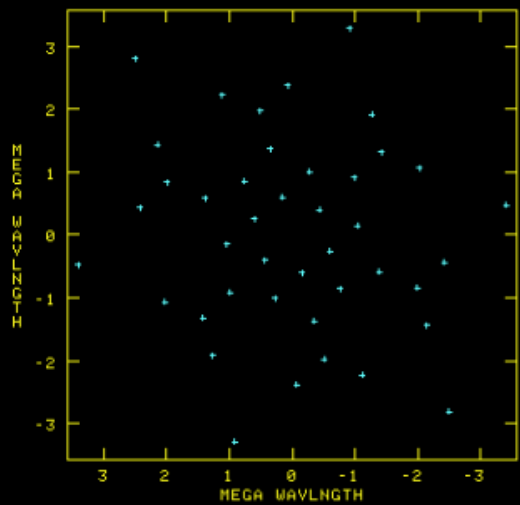
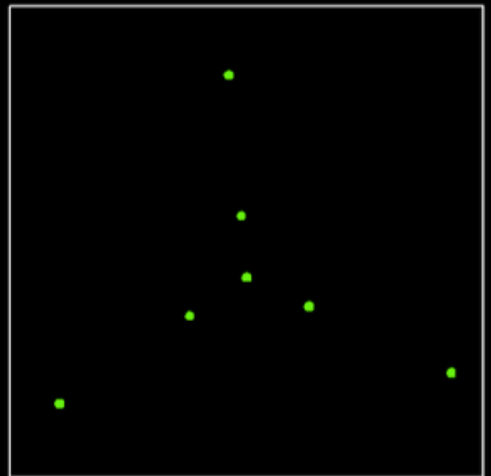


- Separated telescopes (antennas) generate fringes at spatial frequencies where the signal from an object is in phase.
- Increasing the number of telescopes increases the number of baselines, which increases the spatial frequencies sampled partial sampling leads to a complex psf

Telescope locations

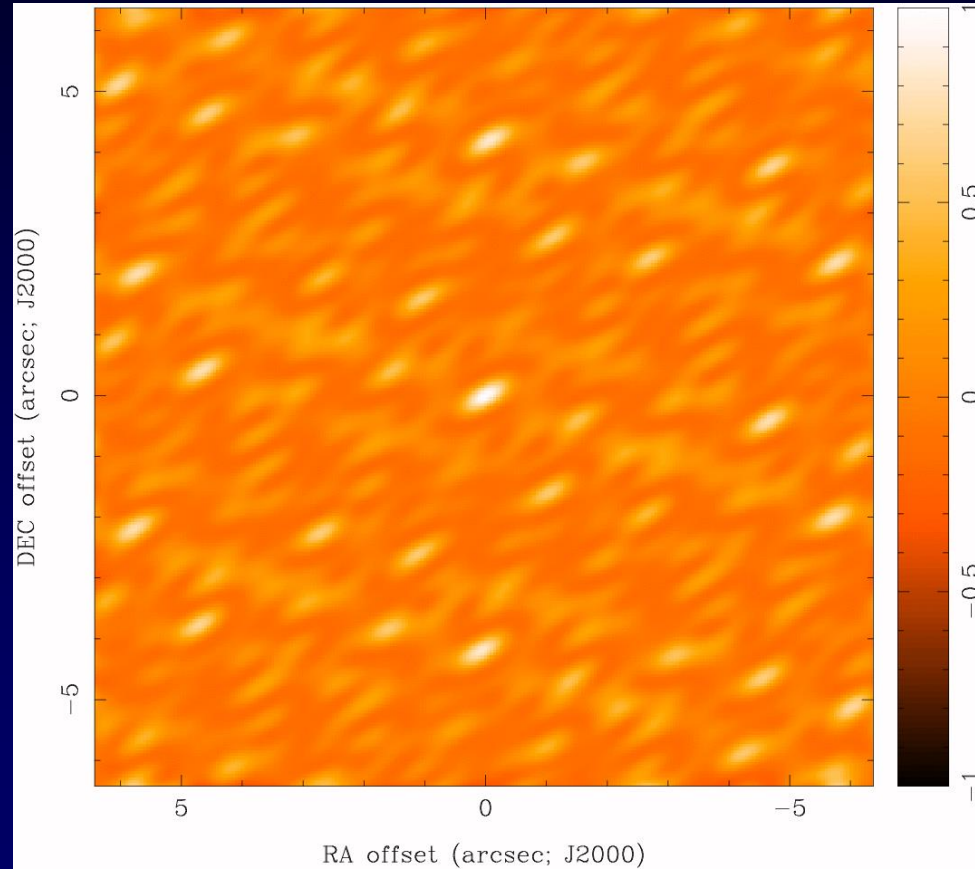
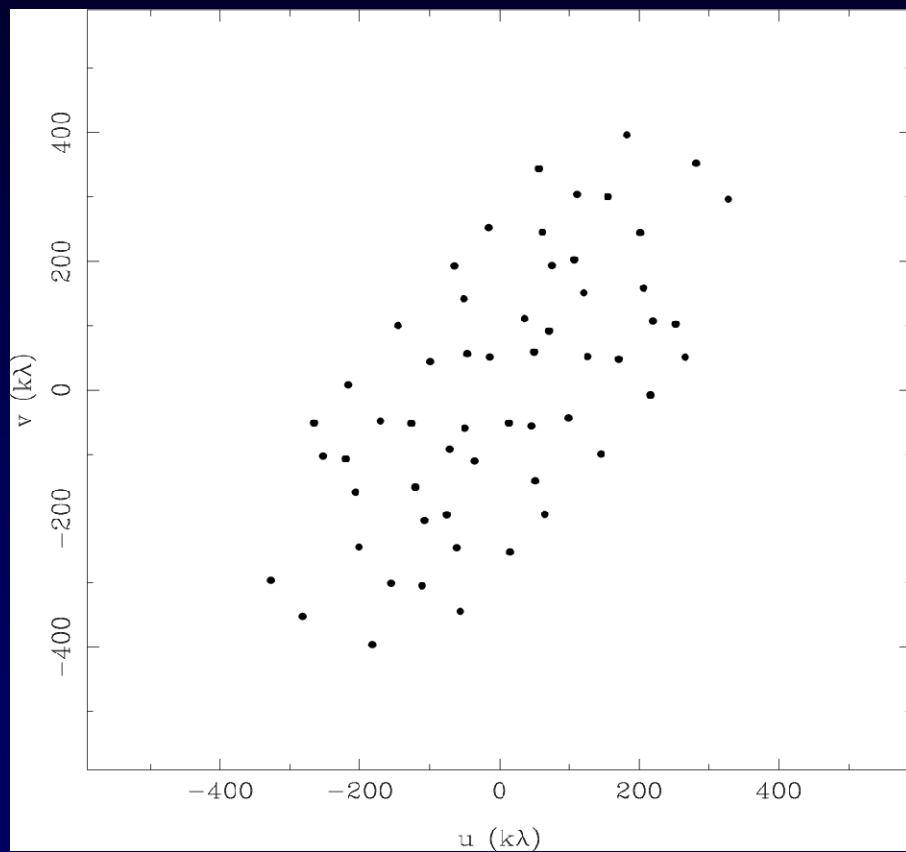
instantaneous uv coverage

PSF



$N(N-1)/2$ baselines

8 Antennas

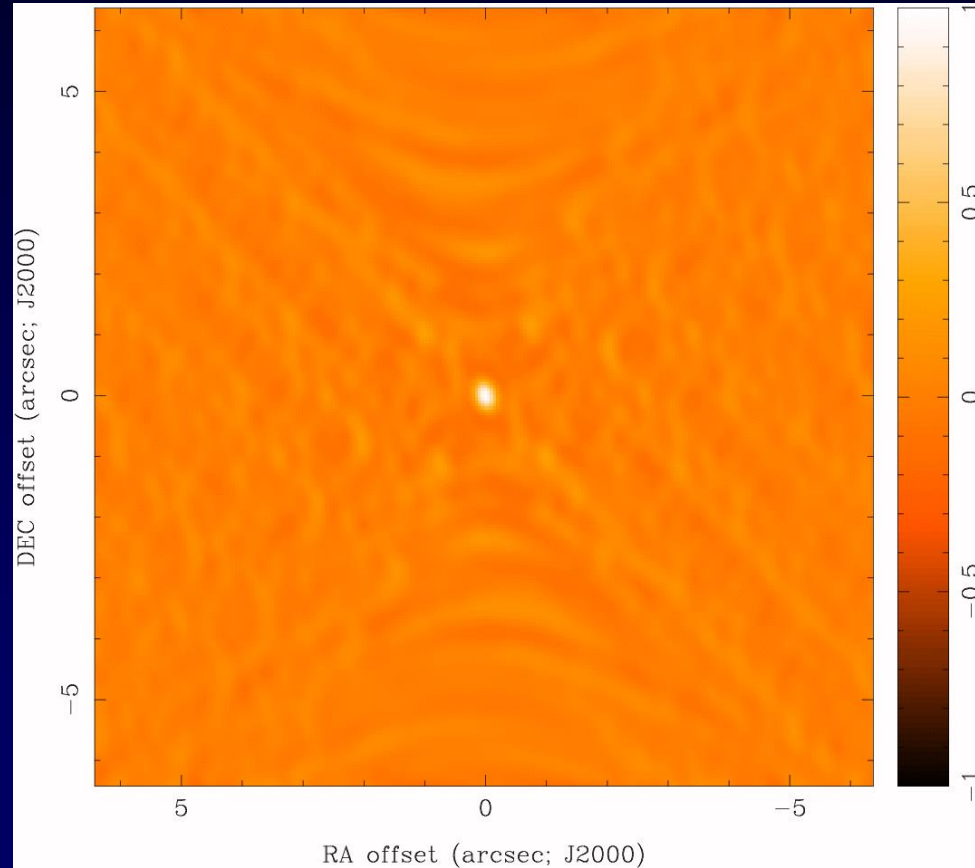
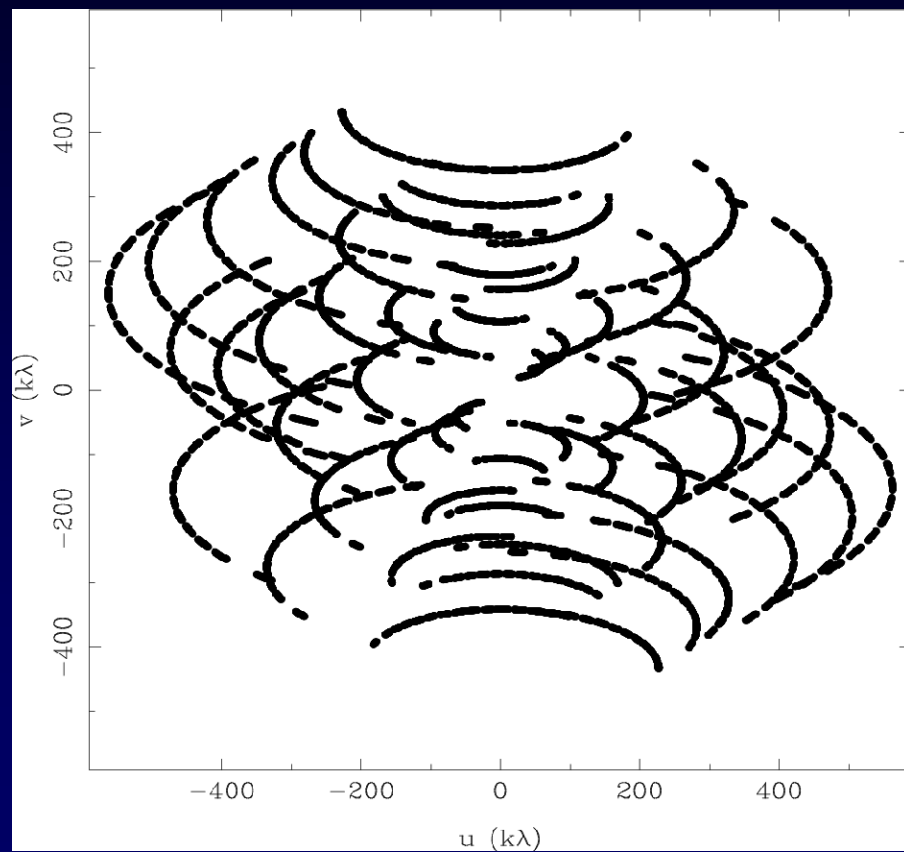


2-D antenna separations

Corresponding image delivered

Effects of Earth's Rotation

8 Antennas x 480 Samples



Increasing the number of baselines sharpens and cleans up the PSF

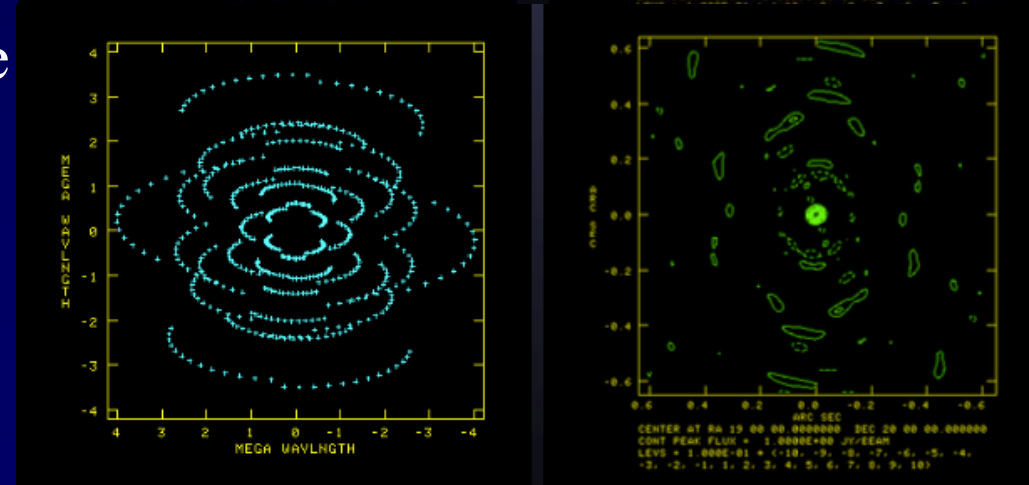
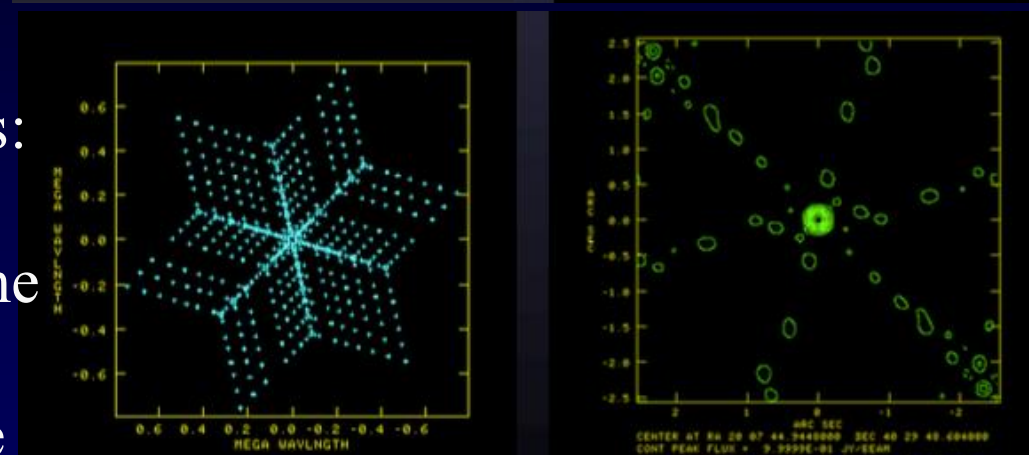
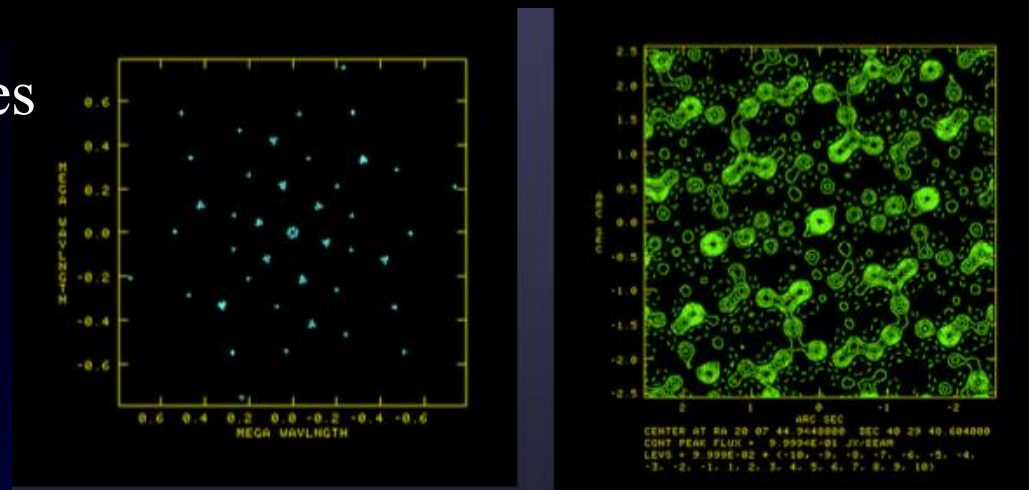
Top – 3 antennas on each arm of the VLA Y configuration

Middle – 8 antennas on each arm

Bottom - Earth rotation synthesis:

As the object moves across the sky, the projected separation of the telescopes changes producing tracks of sampled baselines in the u-v plane (the plane normal to the line of sight to the object, improving sampling and thus the PSF

(Images from C Chandler)



Images from Interferometry

- The signals from the antennas are multiplied together, or correlated, to give fringe amplitudes, which have a $\cos(\phi)$ dependence
- The maximum resolution that can be obtained is given by the maximum baseline, while the maximum scale that is sampled is given by the minimum baseline. Interferometers rarely capture the total flux from an object, and so measurements may need to be complemented by measurements by a single aperture telescope or a more compact configuration (e.g. ALMA has 50 12-m antenna on baseline up to 15km, together with a compact array of 7-m antennas with baselines from 9 to 30 m)
- Note that because of the $\cos(\phi)$ dependence of the interferometer signal, rather than the sinc function of a single antenna, the resolution goes as $\lambda/2b$ rather than λ/D – so masks deployed on a single aperture telescope can increase the resolution.

Radio Frequencies

- $\lambda < 3\text{cm}$ water vapour absorption – need high dry sites
- Between 3cm-50cm atmosphere has little effect on observations (except high winds)
- $\lambda > 50\text{cm}$ ionosphere and solar activity impact observations
 - observations at night are preferred
- Refraction in the troposphere:
 - $n_{\text{air}} = 1.00029$ at $T=0^\circ \text{C}$ and $P=760\text{mm}$ of Hg
 - At radio frequencies water vapour increases dielectric constant and has a substantial effect on the refractive index
 - Effect is the same as at shorter wavelengths, but dispersion is not significant
 - Refractive delay is an important factor in interferometry

Refractive delay

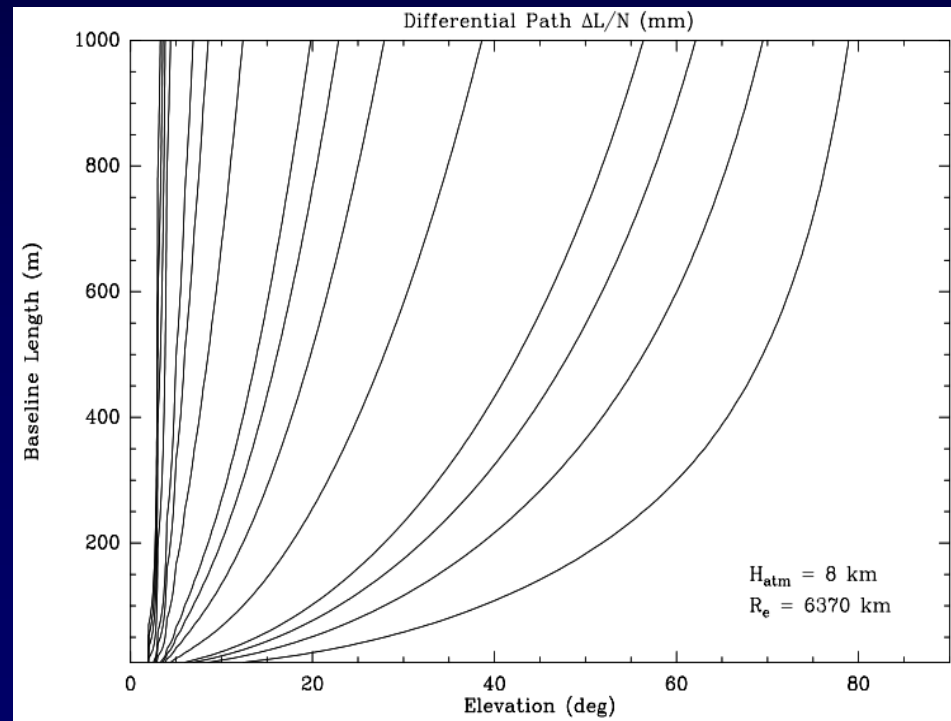
The delay caused by propagation through the atmosphere is the integral of the refractive index along the path

$$t = \int_{r_0}^{\infty} \frac{n(r)}{\sec(z)} dr$$

In practice in interferometry, what matters is the differential delay between different telescopes or antennas.

At IR wavelengths, this can amount to many wavelengths, but for most radio telescopes, Δt is rather small

The figure shows contours of delay as a function of baseline and elevation. The contours are 10, 15, 20, 25, 50, 75, 100, 200, 400, 600, 800, 1000, 3000, and 5000 μm from right to left



mm waves

Wavelengths are $\sim 10^3$ times greater than IR, and dishes are only a bit bigger (ALMA antennas are 12-m)

The whole wavefront suffers retardation, but analysis by E Archibald et al (2002) found no evidence for beam broadening due to seeing at the 15-m JCMT on Mauna Kea

Anomalous refraction can lead to image excursions, possibly due to large scale cells moving over the site

ALMA does not seem to suffer from this, probably because the PWV is lower on Chajnantor



ALMA Phase correction

- Water vapour in the troposphere is not well mixed, leading to large variance of total water vapour column along different lines of sight through the atmosphere [SEP]
- Water vapour is usually described in terms of the column of precipitable water vapour (PWV) above the antenna. The PWV at zenith can vary by a factor of 2 above the ALMA site by as much as 50% over a few minutes
- Water vapour has a high effective refractive index, and 1 mm of PWV retards the incoming wavefront by about 7 mm of path. This is 20λ at ALMA's highest observing frequency
- Radiometers monitor the emission from the 183 GHz water vapour line along the line of sight of the observations, providing estimates of the PWV above each antenna.

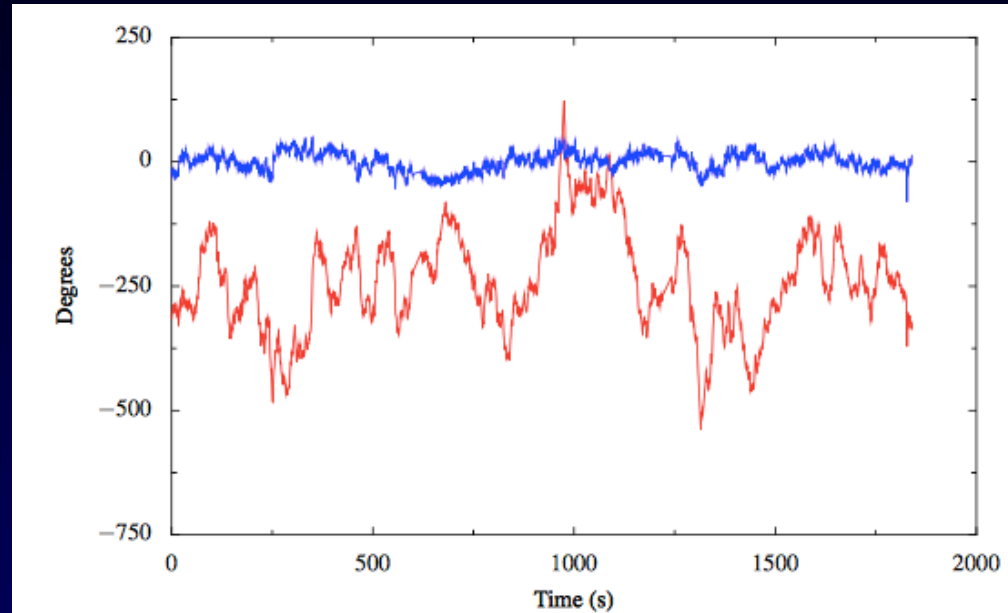


Fig. 8. Test observation at 90 GHz of a strong quasar on a ~650 m baseline with ALMA. The red line is the phase of the observed (complex) visibility on this baseline – note that for a quasar (or other point-like) source at the tracking centre of the interferometer we expect a constant phase in time. The blue line is the visibility phase after correction of the data based on the WVR signals and using the `wvrgcal` program.

Nikolic et al 2013